Article

Series of Fluorescent Dyes Derived from Triphenylamine Structure for Cu²⁺ and In-Cell Carbon Monoxide Sensing: Synthesis and Performance

Yulang Fei, Han Liu, Kai Sun,* and Ou Zhang*

Cite This: ACS Omega 2024, 9, 37737−37747

Read Online

ACCESS | Metrics & More | Article Recommendations | SI Supporting Information

ABSTRACT: In this paper, triphenylamine served as the structural core and was bonded to aromatic groups having various substituents [—OH, —OMe, or —N(Et)₂] by a ═N—N═ chain and then connected with aromatic groups having various substituents [—OH, —OMe, or —N(Et)₂]. The geometric and electronic properties of these probes were examined. It was found that the presence of electron donors enhanced the selectivity and emission quantum yield (QY). When exposed to Cu²⁺, the fluorescence intensity decreased. The optimal probe (T_5) showed a significant decrease in emission QY from 17.1 to 0.5% and recovered to 16.8% after exposure to CO for 342 s. The sensing mechanism was revealed to be static quenching, forming a nonfluorescent adduct between probe and Cu²⁺. After reacting with CO, Cu²⁺ was reduced to Cu⁺, and the probe emission was recovered. The bioimaging performance of the optimal probe was assessed as well.
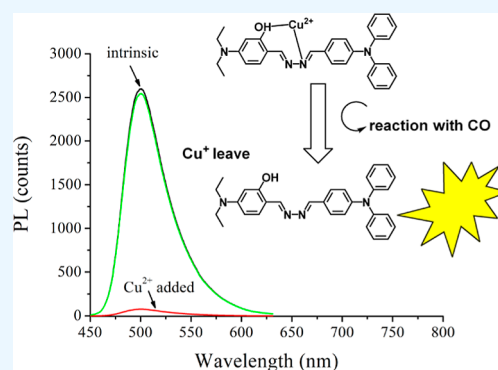
1. INTRODUCTION

As the third most abundant metal ion in the human body, the divalent copper ion (Cu²⁺) plays a key role in various biological reactions, such as serving as a catalytic cofactor of redox-regulating enzymes such as tyrosinase, lysyl oxidase, cytochrome c oxidase, and superoxide dismutase.[1] Both a lack of Cu²⁺ and long-term exposure to high concentrations of Cu²⁺ lead to health problems or diseases.[2−8] For example, an accumulation of Cu²⁺ in the human body leads to reactive oxygen species and thus efficiently damages lipids, DNA, and proteins.[2,3] A high Cu²⁺ concentration in the human body has been associated with various health problems, including Wilson's, Parkinson's, Alzheimer's, Huntington's, and Menkes diseases, and even acute hepatic kidney failure.[4−7] There are many sources of Cu²⁺ release into the environment, such as natural, industrial, and agricultural procedures.[9] The Environmental Protection Agency (EPA) has announced an upper limit of Cu²⁺ in tap water as 20−30 μM and in blood serum as 100−150 μg/dL, making the detection of Cu²⁺ an important task in environmental protection and health care.[10−13]

Among the various candidates for Cu²⁺ detection, optical sensing, which is based on the response of optical signals (fluorescence, absorption, or emission lifetime) to analyte, seems attractive due to its advantages of fast detection, low cost, good selectivity, and easy-to-analysis.[14] There have been examples of optical sensing for Cu²⁺. For example, Kursunlu, Oguz, Yilmaz, and co-workers from the University of Selcuk have developed a series of promising probes based on BODIPY, pillar[5]rene, and isophthalo-NBD for the detection

of metal ions, including Cu²⁺, Sn²⁺, and Hg²⁺. Their further applications such as toxic pollutant removal and bioimaging were developed as well.[15−18] Lin and his research team developed rhodamine-based probes for Cu²⁺.[19] Solid-state sensing of Cu²⁺ has been reported using probe-integrated polymeric sensing materials by Srinivasan and Deivasigamani.[20] Using pyrene-based fluorescent probe, Thirumalaivasan and co-workers developed an optical sensing platform for Cu²⁺.[21] Similarly, Huang and co-workers reported a probe based on pyrene.[22] Meng and co-workers developed an aldazine-based probe for the detection of Cu²⁺.[23] In their work, it was found that the probe emission was first quenched by Cu²⁺, and then, in the presence of a proper reducer such as carbon monoxide (CO), Cu²⁺ was reduced to Cu⁺, with the probe emission well recovered.[22] This finding actually presents a new pathway for the detection of CO. Recent literature have identified endogenic CO as a messenger in signal transduction and therapeutic effects across vital organs such as respiratory, immune, digestive, liver, and kidney systems.[24−26] Consequently, the aforementioned Cu²⁺-probes have found another application in the fluorescence imaging of endogenic CO.[22,23] Generally, to improve photon-harvesting efficiency and
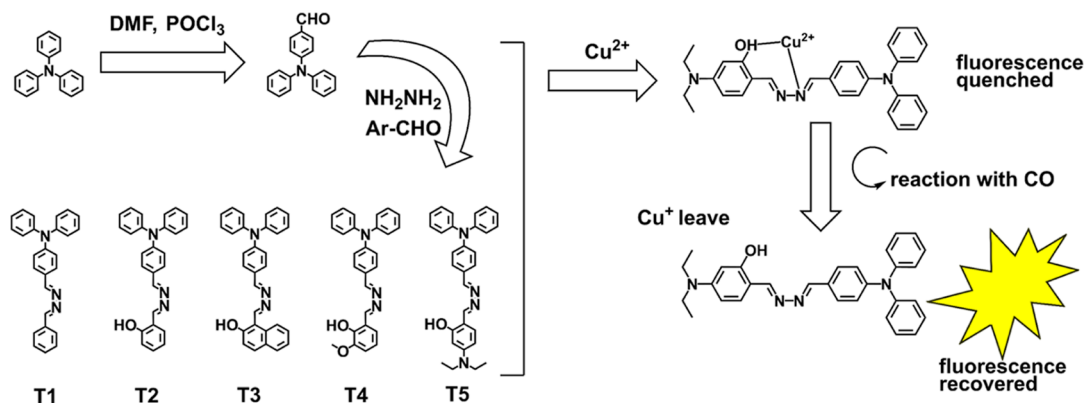
Scheme 1. Synthetic Route and Working Strategy of Five Triphenylamine-Derived Dyes T_n ($n = 1-5$)

decrease energy-wasting structural relaxation in the excited state, the aforementioned Cu^{2+}-probes have large conjugation planes, such as pyrene- and aldazine-derived structures.[21−23] However, it is widely reported that pyrene-like molecules tend to form excimer or exciplex structures due to the $\pi-\pi$ attraction between the coplanar conjugation planes in these probes.[27] The formation of excimer or exciplex structures affects emission wavelength or emission quantum yield (QY), resulting in unexpected results and thus compromising emission-based sensing signals.

To overcome the disadvantage of pyrene-derived probes, in this work, we intend to use triphenylamine as the structural core since triphenylamine has been proven highly luminescent by various literature.[28] As shown in Scheme 1, the triphenylamine group was bonded to an =N—N= chain and then connected to aromatic groups having various substituents [—OH, —OMe, or —N(Et)$_2$]. By comparing their photoluminescence (PL) and sensing performance, the correlation between probe molecular structure and performance can be tentatively clarified. The sensing performance and the sensing mechanism of the optimal probe were reported and discussed, which allowed its further practical application in optical sensing.

2. EXPERIMENT DETAILS

2.1. General Information. Scheme 1 presents the synthetic and working strategies of the five triphenylamine-derived probes reported in this work (denoted as T_1, T_2, T_3, T_4, and T_5), along with their molecular structures. The initial materials and reagents were purchased from Innochem Company in Beijing (China) and with no need for further purification directly for synthesis, including 2-hydroxybenzaldehyde (CAS 90-02-8), 2-hydroxy-1-naphthaldehyde (CAS 708-06-5), 2-hydroxy-3-methoxybenzaldehyde (CAS 148-53-8), 4-(diethylamino)-2-hydroxybenzaldehyde (CAS 17754-90-4), triphenylamine, phosphate buffered saline (PBS), CuCl, CuCl$_2$, and tricarbonylchloro (glycinato) ruthenium(II) (CORM-3). Sample characterization was performed on a Bruker AVANCE 300 spectrometer for nuclear magnetic resonance (NMR) analysis. Single crystal and elemental analyses were performed using a Bruker SMART APEX II X-ray single-crystal diffractometer and a Carlo Erba 1106 elemental analyzer, respectively. Theoretical analysis of the probes was performed by time-dependent density functional theory (TD-DFT) method at the RB3LYP/6-31G(d) level in vacuum using Orca (version 5.04) and Firefly (version 8.2).[29]

The single-crystal structure of the probes (T_2, T_3, T_4, and T_5) was used as the initial geometry. Since we failed to get a T_1 single crystal, we tried to simulate a T_1 structure but the geometry optimization calculation failed to converge. So, the DFT calculation (frontier molecular orbital and absorption simulation) was performed only on T_2, T_3, T_4, and T_5, not on T_1. The frontier molecular orbitals and the simulated absorption spectra were plotted by wxMcMolPlt (version 7.4.4, contour value = 0.03) and Multiwfn (version 3.8, first 50 singlet transitions, broadening function = Gaussian, fwhm = 0.66667 eV), respectively. X-ray photoelectron spectroscopy (XPS) and EPR (electron paramagnetic resonance) experiments were performed using an ESCALAB 250 X-ray photoelectron spectrometer and a Bruker X-band A200 spectrometer, respectively. Fluorescence imaging was carried out using an Olympus FV1200-MPE spectral confocal multiphoton microscope. Absorption and emission spectra were determined in a CH$_3$CN/H$_2$O (v/v = 1:1, 1 μM) solution using a Shimadzu UV-3101PC spectrophotometer and a Hitachi F-7000 fluorescence spectrophotometer (fluorescence mode, 2 × 2 nm). Emission QYs were measured using a literature method with quinine sulfate (in 1.0 M sulfuric acid, Φ_r = 0.546) as a reference.[30] Excited state lifetime was determined by an Edinburgh Instruments F920 spectrometer.

2.2. Synthesis of Triphenylamine-Derived Dyes T_n ($n = 1-5$). 4-(Diphenylamino)benzaldehyde was prepared following a literature method using triphenylamine as the starting material in the presence of DMF (N,N-dimethylformamide) and POCl$_3$.[31] Then, the synthesized 4-(diphenylamino)benzaldehyde (20 mmol) was dissolved in ethanol (40 mL), followed by the slow addition of a mixture of hydrazine hydrate and ethanol (20 mL:20 mL).[32] The resulting solution was stirred at room temperature for 30 min and then at 50 °C for another 8 h. The resulting solid product was collected, washed with ethanol, and dissolved in ethanol (40 mL). To the final solution, the aldehyde compound (20 mmol) was added. The resulting deep red solution was stirred at 75 °C for 10 h. After extracting the solvent under reduced pressure, a brown-yellow solid was collected and purified on an Al$_2$O$_3$ column (FCP 100−200) with petroleum ether/acetic ether (v/v = 100:5) as the eluent. The detailed characterization of T_1−T_5 can be found in Supporting Information.

2.3. Cu^{2+} and CO Sensing Experiment of T_n ($n = 1-5$) via Absorption and Emission Spectra. For the sensing experiment, a mixed solvent of CH$_3$CN/H$_2$O (v/v = 1:1) was
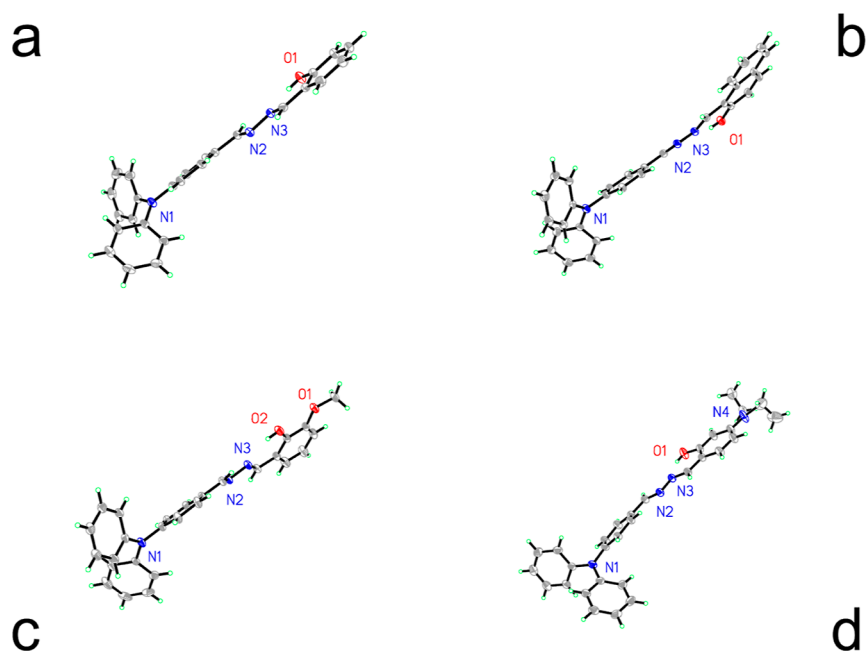
Figure 1. Single-crystal structures of T_2 (a), T_3 (b), T_4 (c), and T_5 (d). H atoms were omitted for clarity. See Supporting Information for full geometric parameters.

applied to ensure good solubility of dyes and various testing reagents (salts, interfering species et al.), despite the fact that this mixed solvent might lead to the degradation or hydrolysis of the dyes, which was mentioned below in Section 3.4.3. T_n dyes were dissolved in CH_3CN/H_2O (v/v = 1:1), then $CuCl_2$ was added and stirred for 2 min before recording the absorption and emission spectra using the aforementioned Shimadzu UV-3101PC spectrophotometer and Hitachi F-7000 fluorescence spectrophotometer (fluorescence mode, slit = 2 × 2 nm). CORM-3 was added and used as a CO source in this work, so that CO concentration could be controlled.[33] No CO bubbles were used in this work to avoid safety threats to crew members and to prevent heterogeneous contact between the T_n solution and the CO stream, which might lead to unexpected and uncontrollable CO concentration distribution in the T_n solution.

2.4. Cell Experiment and Fluorescence Imaging Performance. The cell experiment of selected T_n dyes was conducted with HeLa cells, which first underwent cultivation, measurement, and placement into a 96-well plate for cell culture. Afterward, they were subjected to a 24 h incubation at 37 °C with or without T_n; T_n&Cu^{2+}; and T_n&Cu^{2+}&CORM-3 (with a molar ratio of 1:1:10). Following this, the cells underwent staining using the CCK-8 assay at a wavelength of 450 nm to assess cytotoxicity. Optical density measurements were employed, and Cu^{2+} was introduced as $CuCl_2$.

The performance of selected T_n dyes in the presence of an external CO source, CORM-3, was evaluated. Initially, HeLa cells underwent culture and incubation with T_n&Cu^{2+} (50 μM:50 μM in PBS) for 48 h. Following a PBS wash to eliminate residual T_n&Cu^{2+}, cells were exposed to varying concentrations of CORM-3 (10, 50, and 100 μM) and cultured for 15 min. Subsequently, cells were washed with PBS and subjected to imaging using the Olympus FV1200-MPE spectral confocal multiphoton microscope mentioned earlier. A control experiment was conducted where only T_n&Cu^{2+} was used but no CORM-3 was added.

The endogenous CO imaging performance of selected T_n dyes was evaluated following the procedure described below, which utilized Heme as an internal CO producer. Initially, HeLa cells underwent culture with Heme (100 μM), followed by treatment with T_n&Cu^{2+} (1:1) for 15 min.[34] Subsequent to incubation, the cells were rinsed with PBS, and images were captured using the previously mentioned Olympus FV1200-MPE spectral confocal multiphoton microscope.

3. RESULTS AND DISCUSSION

3.1. Synthesis and Structure of Triphenylamine-Derived Dyes T_n (n = 1−5). As aforementioned, to weaken the $\pi-\pi$ attraction between the coplanar conjugation planes in pyrene-like molecules, triphenylamine was used as the structural core since its three phenylamine rings are non-coplanar with each other, which may partially decrease the possibility of forming excimer or exciplex structures. Then, aromatic rings having various substituents (—OH, —OMe, or —NMe_2) are bonded to the triphenylamine core with an ═N—N═ group so that the correlation between geometric/ electronic substituents and PL/sensing performance can be revealed.

Single crystals were obtained for T_2, T_3, T_4, and T_5, but not for T_1. The unsuccessful preparation of a T_1 single crystal may be explained by the missing phenolic hydroxyl group in T_1, compared to that in T_2, T_3, T_4, and T_5, since a phenolic hydroxyl group increases the molecular dipole moment and thus helps to crystallize. It is observed from Figure 1 that one phenylamine ring from the triphenylamine is nearly coplanar with the aromatic ring, forming a conjugation plane, but the other two phenylamine rings of the triphenylamine are noncoplanar with this conjugation plane. Thus, the size of the conjugation plane in T_1−T_5 is controlled, weakening the $\pi-\pi$ attraction between the coplanar conjugation planes and decreasing the possibility of forming excimer or exciplex structures. This statement is confirmed by the crystal stacking of T_2, T_3, T_4, and T_5. As shown in Figure S1 (Supporting

Information), $\pi-\pi$ stacking is observed in the T_2 crystal but not in the T_3, T_4, and T_5 crystals.

3.2. PET Revealed by Density Functional Theory Calculation in T_n (n = 2−5). It has been reported by Hong and co-workers that there is PET (photoinduced energy transfer) in azobenzene derivatives, and their electronic transitions are sensitive to surrounding factors, such as geometric distortion and coordination with metal ions, showing changes in absorption wavelength, fluorescence wavelength, or intensity. This endows azobenzene derivatives with versatile possibilities of being a probe.[25,26] The first 50 singlet electronic transitions of T_n (n = 2−5) were calculated by TD-DFT at the RB3LYP/6-31G(d) level using their single-crystal structures as the initial geometry. Based on these electronic transitions, their absorption spectra are simulated and compared to their experimentally measured spectra in Figure 2. Two selected orbitals, highest occupied molecular orbital (HOMO) and LUMO (lowest unoccupied molecular orbital), of each T_n (n = 2−5) molecule are plotted and shown
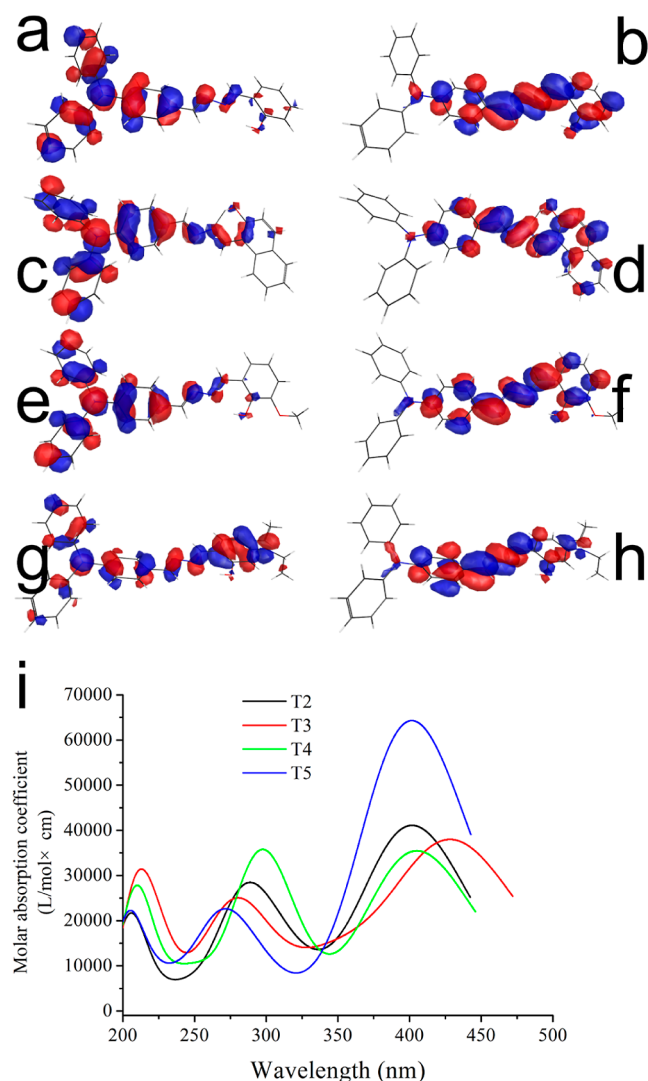
in Figure 2. The HOMO of T_n generally consists of its triphenylamine group, while its LUMO is composed of the ═N—N═C—Ar group. The onset of electronic transition from HOMO to LUMO thus has an obvious electron transfer character. Having an electron-donating group —N(Et)$_2$ in its aromatic ring, T_5 shows the highest transition electric dipole moment value (T^2 = 20.676, see Supporting Information) among these four T_n (n = 2−5) molecules. While the —OMe group in T_4 slightly decreases its transition electric dipole moment value (T^2 = 11.546, see Supporting Information) compared to those of T_2 (T^2 = 13.371, see Supporting Information) and T_3 (T^2 = 12.823, see Supporting Information). It is thus concluded that the —N(Et)$_2$ group increases the electron density of frontier molecular orbitals, which facilitates the PET transition between HOMO and LUMO. But the —OMe group decreases the electron density of frontier molecular orbitals and thus weakens the PET transition between HOMO and LUMO. Upon a structural distortion or transformation, such as coordinating with a metal center, the PET of T_n may be affected, showing spectroscopic signals for optical sensing. This statement will be later confirmed by the experimental result.

3.3. Absorption, Emission, and QY of Intrinsic T_n (n = 1−5). The photophysical parameters of T_n (n = 1−5) are determined and compared in Table 1, including absorption peaks (λ_{abs}), emission peaks (λ_{em}), and emission QYs (ϕ). Figure 3 shows the absorption spectra of T_n (n = 1−5) (in CH$_3$CN/H$_2$O, v/v = 1:1, 2 μM). Due to the rather similar molecular structures of T_n (n = 1−5), these absorption spectra are similar to each other in terms of wavelength and band shape. A slight difference is observed in terms of absorbance. Their multiple absorption bands are comparable to the simulated absorption spectra of T_n (n = 2−5), as shown in Figure 3. Thus, the absorption band of each T_n dye at ~410 nm is attributed to PET absorption. The PET absorption of T_1 is at 404 nm. The incorporation of electron donors (in T_2, T_4, and T_5) or the increased size of the conjugation system (in T_3) leads to a red shift of the PET absorption, as shown in Table 1. T_5 has the highest absorbance among the five T_n dyes, and this result is consistent with its higher transition electric dipole moment value (T^2 = 20.676, see Supporting Information) than those of other T_n (n = 2−5) molecules, as aforementioned in Section 3.2. While the other two absorption bands of each absorption spectrum at ~340 and ~230 nm are mostly preserved, this result means that the PET transition is sensitive to environmental variations and thus can be developed for sensing purpose.

Figure 3 shows the emission spectra of T_n (n = 1−5) (in CH$_3$CN/H$_2$O, v/v = 1:1, 2 μM) and corresponding QYs, along with fwhm (full width at half-maximum) values, which are listed in Table 1. A Gaussian-type single-emission band is observed for each T_n dye. T_1 shows a weak emission peaking at 539 nm with QY of 3.5%. The electron donors in T_2−T_4 shift their emission to longer wavelengths, with QYs slightly increased. The fwhm values of T_1−T_4 are >70 nm, indicating an intense structural relaxation in their excited state, decreasing their emissive energy content and quenching the emissive state, which is confirmed by their limited QYs (lower than 7%). As for T_5, its electron donor [—N(Et)$_2$ group] increases its QY to 17.1%, compared to T_1 (QY = ϕ = 3.5%). However, the emission of T_5 is blue-shifted to 501 nm with fwhm decreased to 49 nm, compared to T_1 (λ_{em} = 539 nm, fwhm = 91 nm), which is consistent with the trend observed in T_2−T_4. There

Figure 2. Frontier molecular orbitals of T_2 (a, HOMO; b, LUMO), T_3 (c, HOMO; d, LUMO), T_4 (e, HOMO; f, LUMO), and T_5 (g, HOMO; h, LUMO), and their simulated absorption spectra (i) calculated at RB3LYP/6-31G(d) level in vacuum (see Supporting Information for singlet electronic transition result).

Table 1. Photophysical Parameters of T_n ($n = 1-5$)

	λ_{abs} (nm)[a]	respond to[b]	λ_{em} (nm)	fwhm (nm)	ϕ (%)	ϕ'[c]	ϕ''[d]	T_{rec} (s)[e]
T_1	404	Cu^{2+}, Fe^{2+}, Fe^{3+}, Hg^{2+}, Ni^{2+}, Zn^{2+}, CO_3^{2-}, PO_4^{3-}, Cys, Hcy	539	91	3.5	1.8	2.2	386
T_2	413	Cu^{2+}	550	72	5.4	0.7	1.6	378
T_3	421	Cu^{2+}, Fe^{3+}, Hg^{2+}	558	87	4.7	1.8	2.4	403
T_4	415	Cu^{2+}, Fe^{2+}, Fe^{3+}, Hg^{2+}, Ni^{2+}, Zn^{2+}, CO_3^{2-}, PO_4^{3-}, Cys, Hcy	547	73	6.8	0.5	5.6	293
T_5	414	Cu^{2+}	501	49	17.1	0.5	16.8	342

[a]PET absorption. [b]Justified by absorption variation, see Section 3.4.1. [c]With the presence of Cu^{2+}(1 equiv). [d]With Cu^{2+}(1 equiv) and CORM-3 (10 equiv). [e]Determined by the time of reaching steady emission (intensity variation <2% within 30 s).
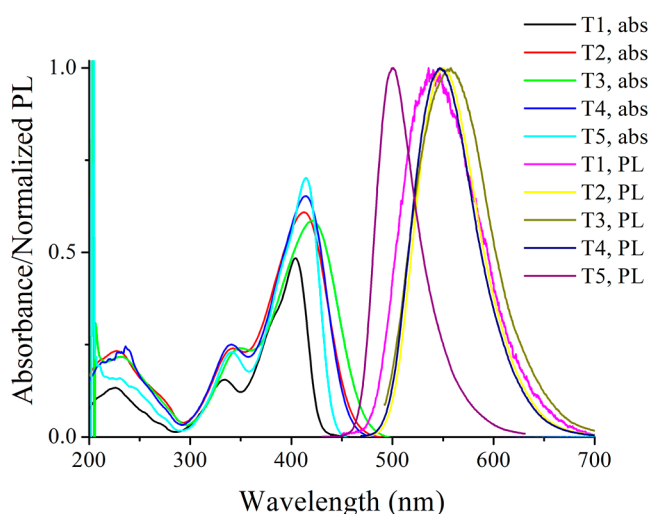

Figure 3. Absorption and normalized PL spectra of T_n in CH_3CN/H_2O (v/v = 1:1, 5 μM).

may be two reasons for the blue-shifted emission of T_5 with decreased fwhm and increased QY: one is the decreased energy loss in the excited state, suggested by the decreased fwhm value of T_5 (compared to T_1), and the other is its high transition electric dipole moment, which allows for an efficient and fast emissive decay of the excited state, suppressing the non-emissive decay (energy loss) of the excited state.

3.4. Sensing Behavior of T_n ($n = 1-5$) Revealed by Absorption and Emission. *3.4.1. Absorption Spectra in the Presence of Cu^{2+} and Competing Species: Selectivity.* To obtain a fast evaluation of their sensing selectivity, the absorption spectra of T_n ($n = 1-5$) in the presence of metal ions, cations, and competing interferents are shown in Figure 4, including Fe^{2+}, Fe^{3+}, Hg^{2+}, Na^+, K^+, Mg^{2+}, Ca^{2+}, Cd^{2+}, Ni^{2+}, Zn^{2+}, Co^{2+}, Mn^{2+}, Sn^{2+}, Cl^-, Br^-, S^{2-}, SO_4^{2-}, NO_3^-, CO_3^{2-}, PO_4^{3-}, Ac^-, ClO^-, glucose, GSH (L-glutathione), Cys (cysteine), and Hcy (homocysteine). Generally speaking, all five T_n dyes are sensitive to Cu^{2+}, with their PET absorption blue-shifted from 410 to 420 nm to 380−390 nm. In addition, the secondary absorption band of free T_n dyes at 330−340 nm disappears after adding Cu^{2+}. This absorption band is assigned as the electronic transition from n (Cl) to π^* (aromatic ring).[35,36] After adding Cu^{2+}, the electron pairs of N atoms coordinated to Cu^{2+} (d orbitals), which explains the disappearance of this absorption band. T_2 and T_5 showed good selectivity since their absorption was blue-shifted by only Cu^{2+}. As for T_3, transition metal ions of Fe^{3+} and Hg^{2+} lead to an absorption blue shift as Cu^{2+} does. As for T_1 and T_4, their absorption blue shift can be triggered by more transition metal ions, anions, and amino acids. Generally speaking, T_1 has the worst selectivity since it has no geometric or electronic factors

to limit ion sensing. The electron donor in T_n improves sensing selectivity, which may be explained by the increased coordination affinity between the ion and T_n, resulting in good selectivities of T_2 and T_5. As for T_3, its enlarged size of the conjugation plane, compared to T_2, spreads the electron distribution and thus weakens the coordination affinity between the ion and T_2, showing worse selectivity. As for T_4, there may be an H-bond between the —OMe group and the —OH group, which weakens the recognition of —OH for metal ions.

3.4.2. Emission Quenching by Cu^{2+}: Spectra and Mechanism. It has been found from Table 1 that T_n ($n = 1-5$) dyes all respond to the same analyte, Cu^{2+}. Thus, we select Cu^{2+} as a quencher to discuss its emission quenching behavior. Figure 5 shows the emission spectra of T_n ($n = 1-5$, 10 μM) with increasing Cu^{2+} concentrations (0−1 equiv). It is observed that all five T_n dyes respond to Cu^{2+} by showing a decreased fluorescence intensity and QYs, as depicted in Figure 5 and Table 1.

As for T_1, T_2, T_4, and T_5, their emission intensity simply decreases with increasing Cu^{2+} concentrations, showing no obvious spectral (blue or red) shift. No shoulder bands or new bands are observed. This result actually suggests a static quenching mechanism: T_n and Cu^{2+} form a nonfluorescent adduct, which decreases the amount of free/fluorescent T_n molecules, leading to a decreased emission intensity. More explanation words are needed for T_3 since it shows a new emission band peaking at 644 nm in the presence of Cu^{2+} (>0.2 equiv). We attribute this emission to the adduct between T_3 and Cu^{2+}. Apparently, the naphthalene ring in T_3 stabilizes the adduct between T_3 and Cu^{2+} and, thus, shows an emission at 644 nm. The other four dyes, T_1, T_2, T_4, and T_5, fail to form a stable and emissive adduct with Cu^{2+}. It is still observed that the linear quenching region of T_4 (0−8 μM) is narrower than those of other four dyes (0−10 μM). A possible reason is that the —OMe group in T_4 offers an additional bonding affinity with Cu^{2+}, especially when Cu^{2+} concentration is high, and thus leads to the nonlinear quenching behavior.

To reveal the sensing mechanism of T_n, the excited state lifetimes (τ) of T_5 in the presence of various Cu^{2+} concentrations are compared and are shown in Figure 5. A monoexponential decay mode is observed for T_5 without Cu^{2+} with a lifetime of 7.1 ns. After increasing the Cu^{2+} concentration to 0.5 and 1.0 equiv, the lifetime is slightly decreased to 6.5 and 6.1 ns. Thus, combined with the aforementioned absorption variation caused by Cu^{2+}, it is concluded that T_n molecules follow a static sensing mechanism toward Cu^{2+}.

After confirming the static sensing mechanism, the fluorescence intensity variation of T_n against Cu^{2+} concentration is analyzed with the Stern−Volmer method.[37] If a luminescent probe follows a dynamic sensing mechanism, its
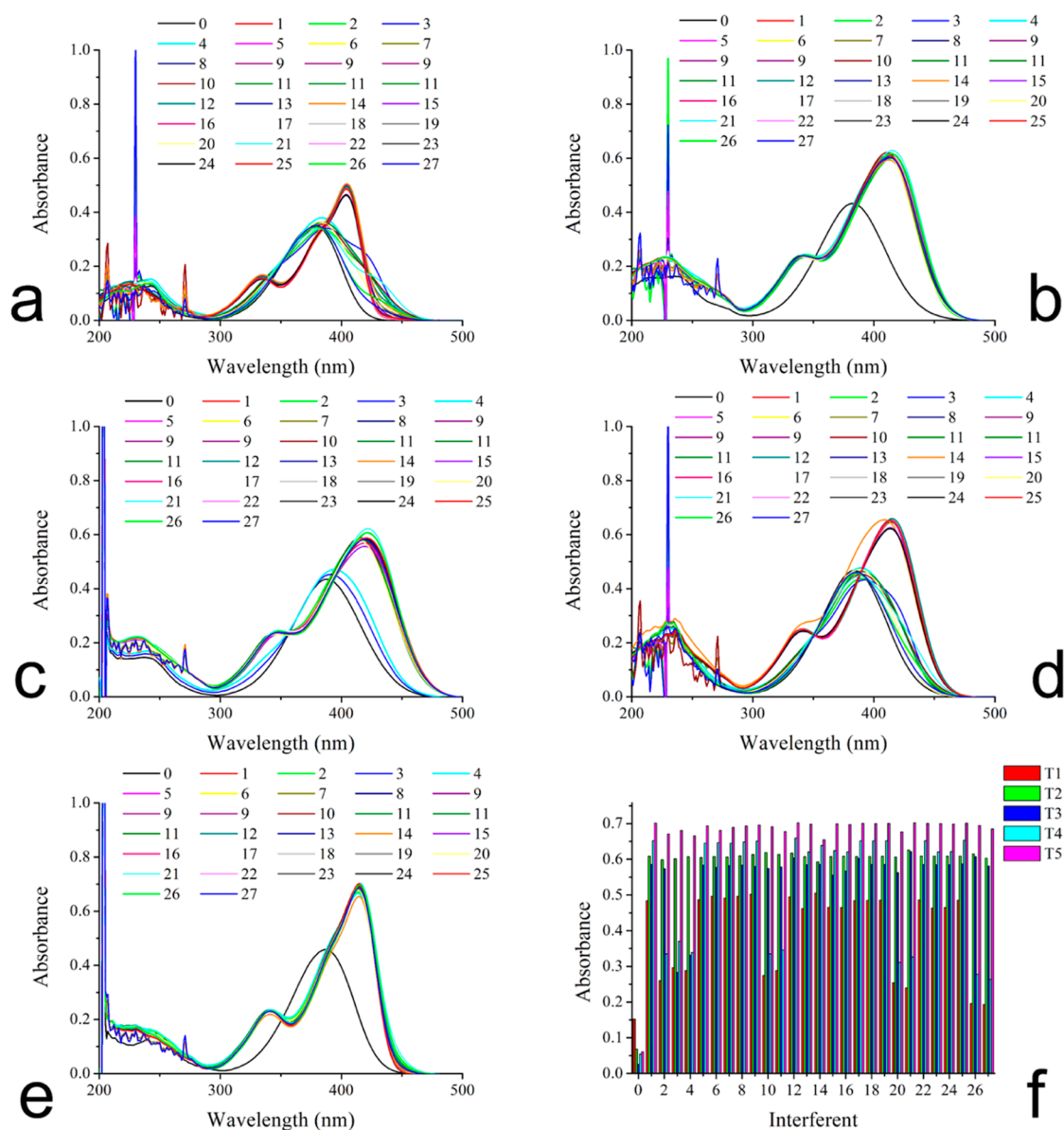
Figure 4. Absorption spectra of T_1 (a), T_2 (b), T_3 (c), T_4 (d), and T_5 (e) in CH_3CN/H_2O (v/v = 1:1, 10 μM) upon the presence of Cu^{2+} (10 μM) and interferents (10 μM) and corresponding PET absorbance variation (f). 0, Cu^{2+}; 1, blank; 2, Fe^{2+}; 3, Fe^{3+}; 4, Hg^{2+}; 5, Na^+; 6, K^+; 7, Mg^{2+}; 8, Ca^{2+}; 9, Cd^{2+}; 10, Ni^{2+}; 11, Zn^{2+}; 12, Co^{2+}; 13, Mn^{2+}; 14, Sn^{2+}; 15, Cl^-; 16, Br^-; 17, S^{2-}; 18, SO_4^{2-}; 19, NO_3^-; 20, CO_3^{2-}; 21, PO_4^{3-}; 22, Ac^-; 23, ClO^-; 24, glucose; 25, GSH; 26, Cys; and 27, Hcy.

emission intensity (F) should follow a linear correlation against quencher concentration [quencher] with a slope of K_{sv}. Here, the subscript 0 means no quencher, K_{sv} is the quenching coefficient, and C is a constant.

$$F_0/F = C + K_{sv}[\text{quencher}] \qquad (1)$$

However, this is not the case shown in Figure 5. Nonlinear curves are observed. On the other hand, the fluorescence intensity of T_n is found to be inversely proportional to the Cu^{2+} concentration. This observation thus finally confirms a static sensing mechanism in T_n toward Cu^{2+}, where T_n forms an adduct with Cu^{2+} and becomes nonfluorescent, leading to a decreased emission intensity.

3.4.3. Emission Stability upon Various Solvents and pH Values. To get a primitive understanding of the emission stability of these fluorescent dyes, the emission spectra of T_1–T_5 are recorded and compared to those after being aged for 7

days in various solvents (CH_2Cl_2, DMF, EtOH, and CH_3CN/H_2O). It is observed from Figure S2 and Table S1 (Supporting Information) that these dyes exhibit an emission red shift after being aged for 7 days, which shall be attributed to the degradation or hydrolysis of the T_n molecules. This red shift tendency is slight in CH_2Cl_2, but it is more obvious in CH_3CN/H_2O, which may be caused by the H_2O molecules that accelerate the hydrolysis or degradation procedures of these dyes. To avoid such hydrolysis and/or degradation procedures, these dyes should be stored in solid state. A low temperature helps to restrain/decrease the hydrolysis and/or degradation procedures, as shown in Figure S3 (Supporting Information). As for the pH effect, T_5 is selected as an example. It is observed from Figure S4 (Supporting Information) that an acidic condition (pH 5.8–7.0) quenches the emission intensity of T_5 and leads to emission blue shift, which originates from the protonation of T_5. While, with the
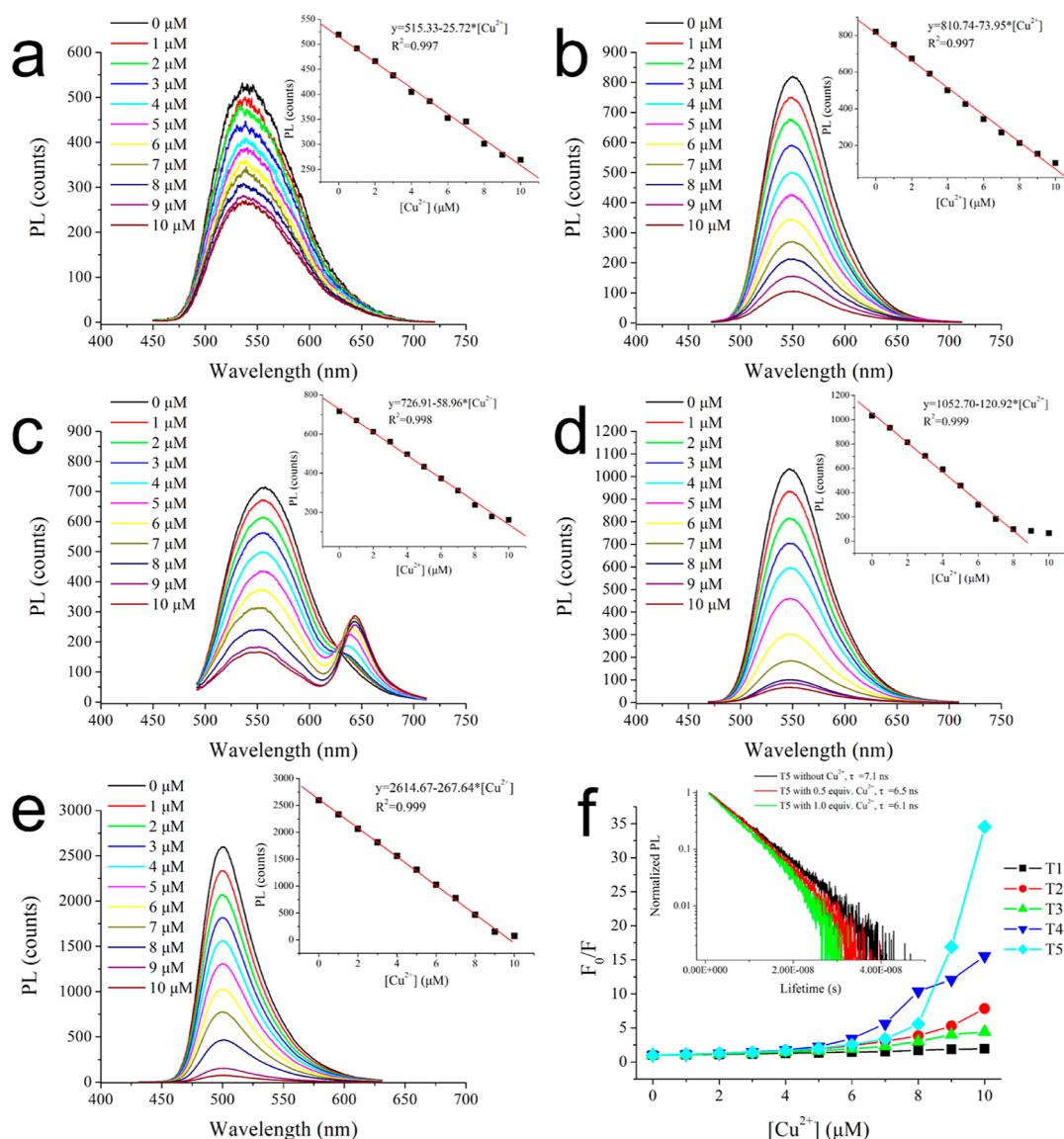
Figure 5. Emission spectra of T_1 (a), T_2 (b), T_3 (c), T_4 (d), and T_5 (e) in CH_3CN/H_2O (v/v = 1:1, 10 μM) upon increasing Cu^{2+} concentrations (0−10 μM); insets: emission intensity variation against $[Cu^{2+}]$ of T_n. Stern−Volmer plots of T_n (f) upon increasing Cu^{2+} concentrations (0−10 μM); inset: excited state lifetime of T_5 upon Cu^{2+} concentrations of 0, 5, and 10 μM.

pH value increased to 7.5, the emission intensity of T_5 is increased, compared to that under pH 7.0, along with an emission red shift, which originates from the deprotonation of T_5 (Ar—OH). An even higher pH value of 8.0, however, tends to quench the emission intensity of T_5. The deprotonation procedure increases the electronic density of T_5 and thus leads to an emission red shift. In the meanwhile, the deprotonated Ar—OH group of T_5 may have severe geometric relaxation, leading to a decreased emission intensity at pH 8.0.

3.5. Emission Recovery of T_n&Cu^{2+} by CORM-3: CO Sensing Potential and Mechanism. It has been aforementioned that T_n forms an adduct with Cu^{2+} and becomes nonfluorescent. Bearing this sensing mechanism in mind, it is assumed that the quenched emission of T_n (in the presence of Cu^{2+}) may be recovered if Cu^{2+} can be removed or replaced. In this work, a carbon monoxide releaser of CORM-3 was introduced, hoping to reduce Cu^{2+} to Cu^+ and thus recover T_n emission.[22] Figure 6 shows emission spectra of T_n&Cu^{2+} (n = 1−5) after adding CORM-3, and their resulting QYs are

determined and listed in Table 1. No surprise, T_n emission is quenched by Cu^{2+}, then, after adding a CO releaser of CORM-3, T_n emission is recovered. The recovered QYs are determined and are listed in Table 1. As for T_1, T_2, and T_3, their recovered emission spectra are similar to their intrinsic emission spectra, with no spectral shifts or new bands, but their recovered QYs are obviously lower than their intrinsic QYs (before adding Cu^{2+}). As for T_4 and T_5, their recovered QYs are close to their intrinsic QYs (before adding Cu^{2+}), and their recovered emission spectra are rather similar to those of their intrinsic emission spectra. This result suggests a reversible formation and/or dissociation of the adduct between T_4/T_5 and Cu^{2+}. The difference in emission recovery between T_1/T_2/ T_3 and T_4/T_5 is tentatively attributed to the electron donors in T_4 and T_5.

The time-resolved emission recovery of T_n (n = 1−5) is revealed by monitoring their emission intensity after adding CORM-3. As shown in Figure 6, a low emission intensity is observed for each T_n&Cu^{2+} sample. After the addition of
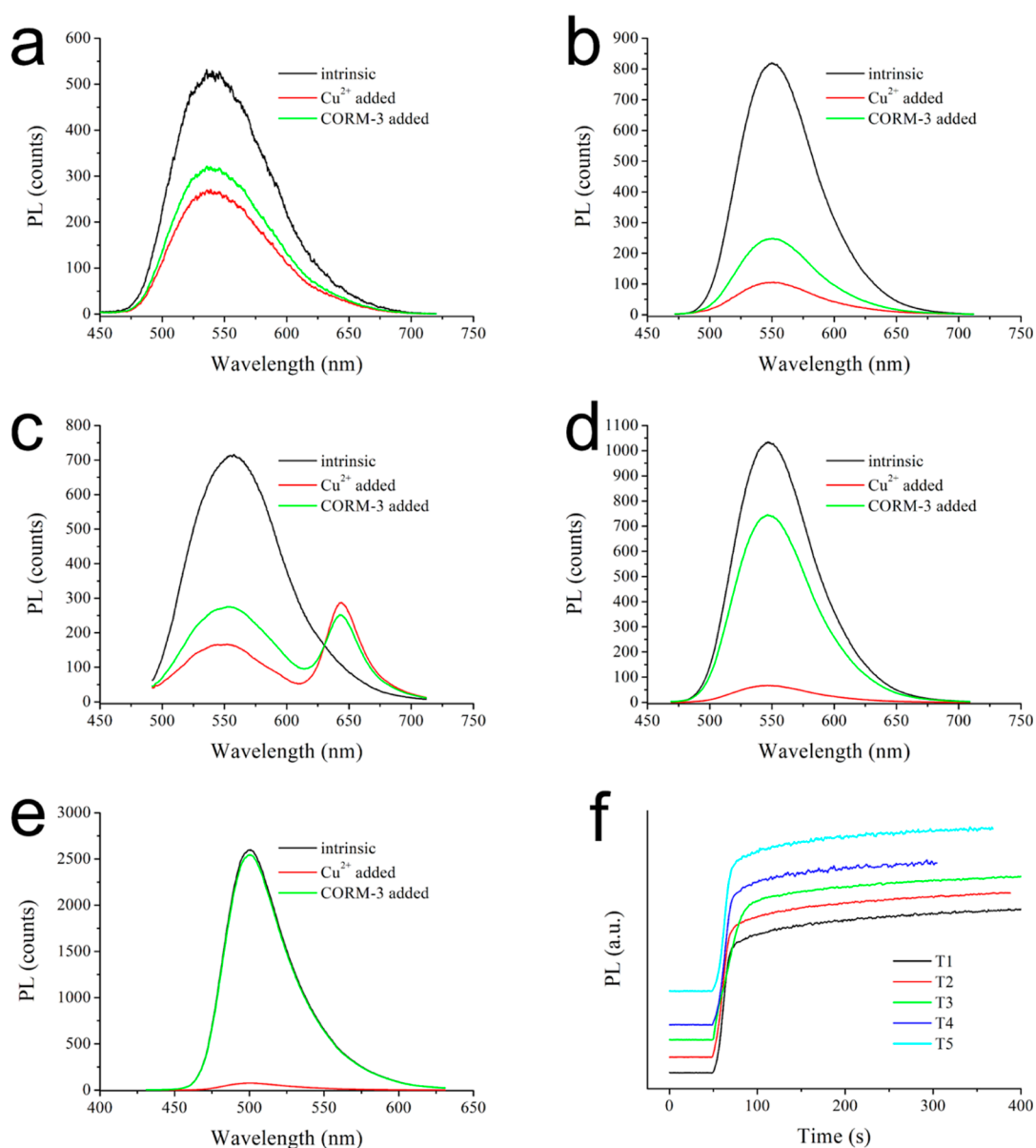
Figure 6. Emission spectra of intrinsic T_n, $T_n\&Cu^{2+}$ ($n = 1-5$), and $T_n\&Cu^{2+}$ ($n = 1-5$) after adding CORM-3, T_1 (a), T_2 (b), T_3 (c), T_4 (d), and T_5 (e). Emission intensity monitoring of $T_n\&Cu^{2+}$ ($n = 1-5$) after adding CORM-3 (f).

CORM-3, the emission intensity increases instantly and finally remains stable. For convenience of comparison, the recovery time (T_{rec}) is defined as the time for each $T_n\&Cu^{2+}$ sample to reach steady emission (intensity variation <2% within 30 s). Generally, it is found that the electron donors in T_2, T_3, and T_5 decrease their emission recovery time compared to T_1. T_3 shows the longest recovery time among the five T_n dyes, which may be attributed to the steric hindrance of the anthracene group.

For a better understanding of the formation of T_n and Cu^{2+}, two dyes (T_2 and T_5), which have different recovery behaviors, are selected, and the complexation constant (K) of $T_2\&Cu^{2+}$ is calculated by eq 2 and compared with that of $T_5\&Cu^{2+}$. The total concentration of T_2/T_5 and Cu^{2+} is fixed as 10 μM, and an absorption titration is performed.[38] Here, A is the recorded maximum absorbance, A' is the theoretical absorbance, and α is dissociation ratio.

$$T_2/T_5 + Cu^{2+} = T_2/T_5\&Cu^{2+} \quad (2)$$

$$\alpha = (A' - A)/A' \quad (3)$$

$$K = (1 - \alpha)/\{[T_2/T_5\&Cu^{2+}]\alpha^2\} \quad (4)$$

It is observed from Figure 7 that the absorbance of T_2 and T_5 reaches the maximum value at a $[Cu^{2+}]/\{[Cu^{2+}] + [T_n]\}$ molar ratio of 50%, which means a 1:1 stoichiometric ratio between Cu^{2+} and T_2/T_5. The K value of T_2 is determined as 1.635×10^9 L/mol, while that of T_5 is 2.970×10^7 L/mol. Apparently, T_2 has a higher coordination affinity with Cu^{2+} and forms a more stable adduct than T_5. As a consequence, T_2 shows poor emission recovery after adding CORM-3, but T_5 shows good emission recovery after adding CORM-3.

The emission recovery mechanism of $T_n\&Cu^{2+}$ by CORM-3 is tentatively discussed by a comparative XPS study. It is observed from Figure 7 that $T_5\&Cu^{2+}$ renders an XPS peak of 934.0 eV, corresponding to Cu^{2+}, along with a shoulder XPS peak of 933.0 eV corresponding to Cu^{2+}, as previously reported by a literature.[39] After the addition of CORM-3, the XPS
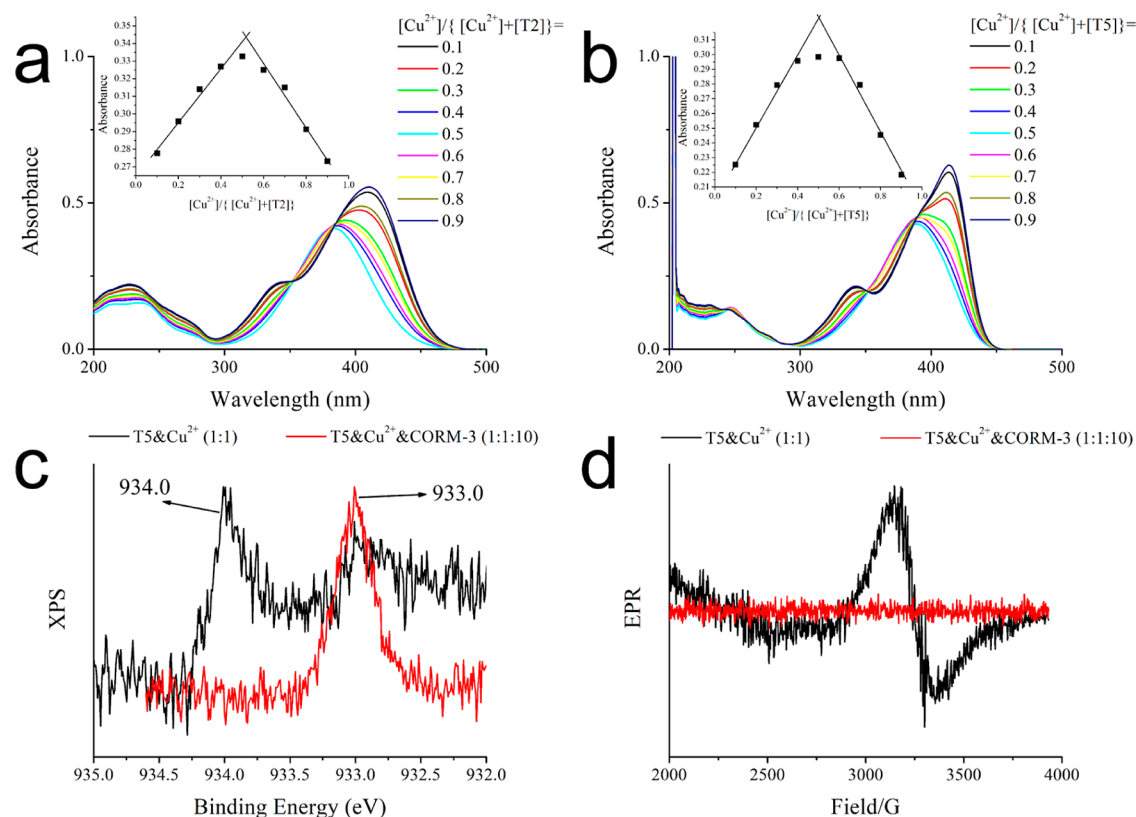
Figure 7. Absorption titration spectra of T_2 (a) and T_5 (b). XPS spectra (c) and EPR result (d) of T_5&Cu^{2+} (1:1) and T_5&Cu^{2+}&CORM-3 (1:1:10).

intensity at 934.0 eV disappears, while that at 933.0 eV is clearly observed. This result suggests that Cu^{2+} has been reduced to Cu^{2+} by CORM-3. This statement is further confirmed by a comparative EPR (electron paramagnetic resonance) study. As shown in Figure 7, a typical EPR signal is observed for T_5&Cu^{2+}, which matches the empty d orbitals (d^9) in Cu^{2+}.[40] After the addition of CORM-3, the EPR signal disappears, indicating the full d^{10} orbitals in Cu^+.

3.6. Cytotoxicity and Exogenous and Endogenous CO Imaging with T_5. After comparison of the five T_n dyes in terms of selectivity, fluorescence QYs, and emission recovery, T_5 is found to be superior to the other four dyes and is thus selected for the following cell experiment. The disadvantages of T_1, T_3, and T_4 are their poor selectivity, while T_2 shows poor emission recovery in the presence of CO. T_5 has good selectivity and obvious change of QYs (with Cu^{2+} or with CO) due to its suitable size of conjugation plane and substituents [—OH and —N(Et)$_2$]. First, its cell viability testing is performed to evaluate its potential in bioimaging. As shown in Figure 8, a cell viability rate of 98.0% is observed in the presence of 10 μM T_5 and then decreases with increasing T_5 concentrations. At a T_5 concentration of 100 μM, the cell viability decreased to 63.2%.

By addition of Cu^{2+} and CORM-3, the cell viability further drops to 56.1% (with Cu^{2+}, 1:1) and 52.4% (with Cu^{2+} and CORM-3, 1:1:10), respectively. For the following experiment, T_5 concentration is fixed as 50 μM to ensure cell viability. Then, the exogenous CO imaging performance of T_5 is discussed using HeLa cells and CORM-3 as a CO source. No detectable emission is observed when only T_5&Cu^{2+} is added. By increasing the CORM-3 concentrations to 20, 50, and 100 μM, the green emission becomes stronger and stronger,

indicating a cell endocytosis process for CORM-3. Thus, exogenous CO imaging using CORM-3 has been confirmed. Then, using Heme as the endogenous CO source, the CO imaging performance of T_5 is further revealed as follows. In the absence of Heme, no detectable emission signal is observed. After adding Heme (100 μM) to HeLa cells, the Heme metabolic process releases CO for T_5 imaging.[26] It is observed from Figure 8 that the green emission becomes stronger and stronger as the reaction time increases, confirming the endogenous CO imaging of T_5 with the help of Cu^{2+}.

4. CONCLUSIONS

In summary, this work reported five probes derived from triphenylamine with various substituents [—OH, —OMe, or —N(Et)$_2$], including their synthesis, geometric structure, electronic transitions, comparison of photophysical properties (with or without Cu^{2+}), and potential application in bioimaging. It was found that the electron donors in these probes improved selectivity and emission QY. T_5 showed superior performance over the other four dyes. Its QY was quenched from 17.1 to 0.5% by Cu^{2+} and recovered to 16.8% after an exposure to CO within 342 s. T_5 followed a static sensing mechanism by forming a nonfluorescent adduct with Cu^{2+}. CO reduced Cu^{2+} to Cu^+ and, thus, recovered T_5 emission. The bioimaging performance of the optimal probe was evaluated as well. The novelty of these triphenylamine-based probes was that they showed no obvious influence from intermolecular $\pi-\pi$ attraction, compared to the pyrene-based probes. The disadvantage of T_5 was its unsatisfactory cell cytotoxicity. For future efforts, more similar probes with low cell cytotoxicity should be synthesized and tested. In addition,
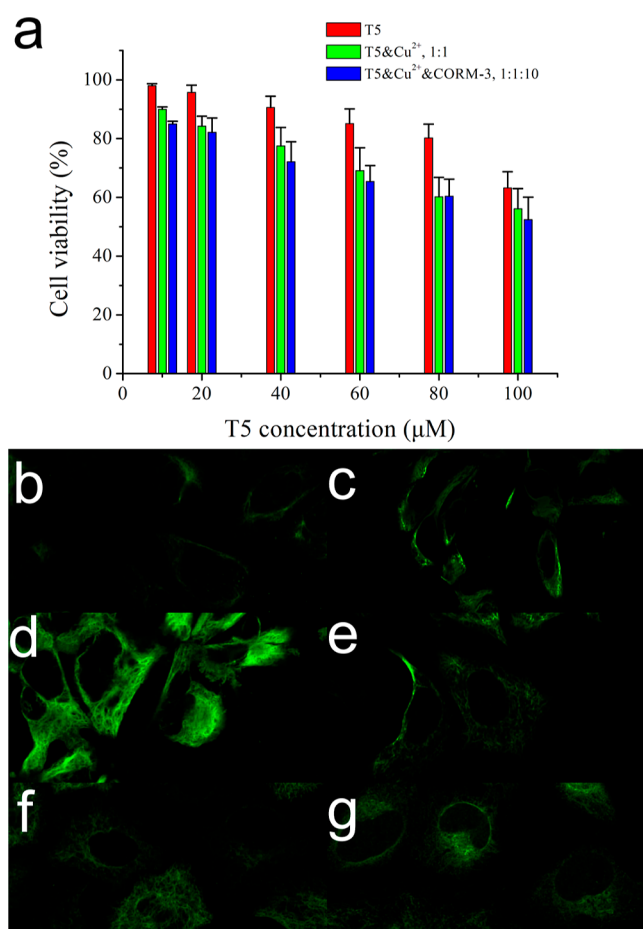
Figure 8. Cell cytotoxicity of T_5 (a), bioimaging photos of HeLa cells without and with CORM-3 (b, 10; c, 30; and d, 100 μM), and HeLa cells with Heme upon various hours (e, 0.5; f, 1; and g, 2 h).

these fluorescent dyes in their present form are not suitable for gaseous CO sensing since they are dispersed in aqueous-based solutions or in condensed state. In aqueous-based solutions, the gaseous CO has a rather low solubility (0.0026 g/100 g), which makes the CO sensing in aqueous-based solutions meaningless (more or less). In condensed state, the gaseous CO can hardly penetrate the dyes in solid state, leading to sensing behavior only on solid surface and thus poor sensing performance. To apply these dyes for the sensing of gaseous CO, they should be dispersed or embedded or immobilized in a solid but porous host, which allows the fluent transportation of gaseous CO.

ASSOCIATED CONTENT

Ⓢ Supporting Information

The Supporting Information is available free of charge at https://pubs.acs.org/doi/10.1021/acsomega.4c03137.

Characterization details and ^{1}H NMR spectra of T_1–T_5; photo of T_5 upon excitation wavelength of 414 nm; emission spectra of T_1–T_5 before and after being aged for 7 days in various solvents; emission spectra of T_5 before and after being stored for 7 days at 4 and 35 °C; emission spectra of T_5 in CH_3CN/H_2O solutions (10 μM) with various pH values (5.8–8.0); TD-DFT result of T_2-T_5 calculated at RB3LYP/6-31G(d) level in vacuum; packing mode of T_2–T_5 crystals; and crystal details and full geometric parameters of T_2–T_5 (PDF)

AUTHOR INFORMATION

Corresponding Authors

Kai Sun − *The First Affiliated Hospital of Nanyang Medical College, Nanyang 473061 Henan Province, China;* ⊙ orcid.org/0009-0004-7138-781X; Email: sunkai796@163.com

Ou Zhang − *The First Affiliated Hospital of Nanyang Medical College, Nanyang 473061 Henan Province, China;* ⊙ orcid.org/0009-0006-5769-4287; Email: zhangou361@163.com

Authors

Yulang Fei − *Department of Biomedical Research Center, Medical College, Xijing University, Xi 'an 710123 Shaanxi Province, China; The First Affiliated Hospital of Nanyang Medical College, Nanyang 473061 Henan Province, China*

Han Liu − *Department of the Spleen and Stomach Diseases, Xi'an Hospital of Traditional Chinese Medicine, Xi 'an 710000 Shaanxi Province, China*

Complete contact information is available at:
https://pubs.acs.org/10.1021/acsomega.4c03137

Notes

The authors declare no competing financial interest.

REFERENCES

(1) Gerdan, Z.; Saylan, Y.; Denizli, A. Recent Advances of Optical Sensors for Copper Ion Detection. *Micromachines* **2022**, *13*, 1298.

(2) Sakunkaewkasem, S.; Petdum, A.; Panchan, W.; Sirirak, J.; Charoenpanich, A.; Sooksimuang, T.; Wanichacheva, N. Dual-Analyte Fluorescent Sensor Based on [5]Helicene Derivative with Super Large Stokes Shift for the Selective Determinations of Cu^{2+} or Zn^{2+} in Buffer Solutions and Its Application in a Living Cell. *ACS Sens.* **2018**, *3*, 1016−1023.

(3) Abu-Dalo, M. A.; Salam, A. A.; Nassory, N. S. Ion Imprinted Polymer Based Electrochemical Sensor for Environmental Monitoring of Copper(II). *Int. J. Electrochem. Sci.* **2015**, *10*, 6780−6793.

(4) Tarnowska, M.; Krawczyk, T. Click chemistry as a tool in biosensing systems for sensitive copper detection. *Biosens. Bioelectron.* **2020**, *169*, 112614.

(5) Nadimetla, D. N.; Bhosale, S. V. Tetraphenylethylene AIEgen bearing thiophenylbipyridine receptor for selective detection of copper(ii) ion. *New J. Chem.* **2021**, *45*, 7614−7621.

(6) Kuras, M. J.; Więckowska, E. Synthesis and characterization of a new copper(II) ion-imprinted polymer. *Polym. Bull.* **2015**, *72*, 3227−3240.

(7) Shen, Y. J.; Zhang, K. A bifunctional optical probe based on ESIPT-triggered disalicylaldehyde with ratiometric detection of iron and copper ions. *Polyhedron* **2021**, *193*, 114883.

(8) Kirk, K. A.; Andreescu, S. Easy-to-Use Sensors for Field Monitoring of Copper Contamination in Water and Pesticide-Sprayed Plants. *Anal. Chem.* **2019**, *91*, 13892−13899.

(9) U.S. Environmental Protection Agency Office of Pesticide Programs. *Copper Facts*; USEPA: New York, NY, USA, 2008; pp 1−35.

(10) Yuan, Z.; Cai, N.; Du, Y.; He, Y.; Yeung, E. S. Sensitive and Selective Detection of Copper Ions with Highly Stable Polyethyle-

neimine-Protected Silver Nanoclusters. *Anal. Chem.* **2014**, *86*, 419−426.

(11) Adi Narayana Reddy, S.; Reddy, K. J.; Duk, L. K.; Reddy, A. V. Evaluation of 2,6-diacetylpyridinebis-4-phenyl-3-thiosemicarbazone as complexing reagent for zinc in food and environmental samples. *J. Saudi Chem. Soc.* **2016**, *20*, S271−S279.

(12) Kong, T.; Liu, G. W.; Li, X. B.; Wang, Z.; Zhang, Z. G.; Xie, G. H.; Zhang, Y.; Sun, J.; Xu, C. Synthesis and identification of artificial antigens for cadmium and copper. *Food Chem.* **2010**, *123*, 1204−1209.

(13) Zhao, Z.; Chen, H.; Zhang, H.; Ma, L.; Wang, Z. Polyacrylamide-phytic acid-polydopamine conducting porous hydrogel for rapid detection and removal of copper (II) ions. *Biosens. Bioelectron.* **2017**, *91*, 306−312.

(14) Pirzada, M.; Altintas, Z. Recent Progress in Optical Sensors for Biomedical Diagnostics. *Micromachines* **2020**, *11*, 356.

(15) Bilgic, A.; Cimen, A.; Kursunlu, A. N. "Killing two birds with one stone": A fluorescent hybrid nanoparticle modified with BODIPY for efficiently detection and removal of toxic Cu (II) ion from aqueous solutions. *Sci. Total Environ.* **2022**, *845*, 157170.

(16) Kursunlu, A. N.; Bastug, E.; Oguz, A.; Oguz, M.; Yilmaz, M. A highly branched macrocycle-based dual-channel sensor: Bodipy and pillar[5]arene combination for detection of Sn (II) &Hg (II) and bioimaging in living cells. *Anal. Chim. Acta* **2022**, *1196*, 339542.

(17) Oguz, M.; Gul, A.; Kursunlu, A. N.; Yilmaz, M. A bifunctional and multi-responsive fluorescent sensor for toxic analytes in the aqueous medium: Easy synthesis, NIR-visible effect, imaging in living cells. *J. Mol. Liq.* **2021**, *336*, 116861.

(18) Bilgic, A.; Cimen, A.; Bagtug, E.; Kursunlu, A. N. Fluorescent sporopollenin microcapsule modifiedby BODIPY for sensitive&selective recognition andefficient removal of Cu (II) from aqueous solution. *Chem. Eng. Res. Des.* **2022**, *178*, 61−72.

(19) Arumugaperumal, R.; Srinivasadesikan, V.; Lin, M. C.; Shellaiah, M.; Shukla, T.; Lin, H. C. Facile rhodamine-based colorimetric sensors for sequential detections of Cu(ii) ions and pyrophosphate ($P_2O_7^{4-}$) anions. *RSC Adv.* **2016**, *6*, 106631−106640.

(20) Srinivasan, P.; Deivasigamani, P. Solid-state naked-eye sensing of Cu(II) from industrial effluents and environmental water samples using probe integrated polymeric sensor materials. *Microchem. J.* **2023**, *185*, 108224.

(21) Shellaiah, M.; Venkatesan, P.; Thirumalaivasan, N.; Wu, S. P.; Sun, K. W. Pyrene-Based Fluorescent Probe for "Off-on-Off" Sequential Detection of Cu^{2+} and CN^- with HeLa Cells Imaging. *Chemosensors* **2023**, *11*, 115.

(22) Bai, C.; Zhang, J.; Qin, Y.; Meng, Q.; Yao, J.; Huang, H.; Wei, B.; Li, R.; Zhang, L.; Miao, H.; Qu, C.; Qiao, R. Strategy for Detecting Carbon Monoxide: Cu^{2+}-Assisted Fluorescent Probe and Its Applications in Biological Imaging. *Anal. Chem.* **2022**, *94*, 11298−11306.

(23) Jia, H.; Yang, M.; Meng, Q.; He, G.; Wang, Y.; Hu, Z.; Zhang, R.; Zhang, Z. Synthesis and Application of an Aldazine-Based Fluorescence Chemosensor for the Sequential Detection of Cu^{2+} and Biological Thiols in Aqueous Solution and Living Cells. *Sensors* **2016**, *16*, 79.

(24) Morstein, J.; Höfler, D.; Ueno, K.; Jurss, J. W.; Walvoord, R. R.; Bruemmer, K. J.; Rezgui, S. P.; Brewer, T. F.; Saitoe, M.; Michel, B. W.; Chang, C. J. Ligand-Directed Approach to Activity-Based Sensing: Developing Palladacycle Fluorescent Probes That Enable Endogenous Carbon Monoxide Detection. *J. Am. Chem. Soc.* **2020**, *142*, 15917−15930.

(25) Hong, J.; Xia, Q.; Zhou, E.; Feng, G. NIR fluorescent probe based on a modified rhodol-dye with good water solubility and large Stokes shift for monitoring CO in living systems. *Talanta* **2020**, *215*, 120914.

(26) Yan, H.; Du, J.; Zhu, S.; Nie, G.; Zhang, H.; Gu, Z.; Zhao, Y. Emerging Delivery Strategies of Carbon Monoxide for Therapeutic Applications: from CO Gas to CO Releasing Nanomaterials. *Small* **2019**, *15*, 1904382.

(27) Jung, H. S.; Park, M.; Han, D. Y.; Kim, E.; Lee, C.; Ham, S.; Kim, J. S. Cu^{2+} Ion-Induced Self-Assembly of Pyrenylquinoline with a Pyrenyl Excimer Formation. *Org. Lett.* **2009**, *11*, 3378−3381.

(28) Zhang, L.; Li, B. A series of Eu(III) emitters with a novel triphenylamine-derived beta-diketone ligand. *J. Lumin.* **2009**, *129*, 1304−1308.

(29) Jorge, F. E.; Jorge, S. S.; Suave, R. N. Electronic Circular Dichroism of Chiral Alkenes: B3LYP and CAM-B3LYP Calculations. *Chirality* **2015**, *27*, 23−31.

(30) Ye, K.; Wang, J.; Sun, H.; Liu, Y.; Mu, Z.; Li, F.; Jiang, S.; Zhang, J.; Zhang, H.; Wang, Y.; Che, C. Supramolecular structures and assembly and luminescent properties of quinacridone derivatives. *J. Phys. Chem. B* **2005**, *109*, 8008−8016.

(31) Yang, Y.; Li, B.; Zhang, L. Design and synthesis of triphenylamine-malonitrile derivatives as solvatochromic fluorescent dyes. *Sens. Actuators, B* **2013**, *183*, 46−51.

(32) Ghosh, A.; Adhikari, S.; T, S.; Banik, A.; Dangar, T. K.; Mukhopadhyay, S. K.; Matalobos, J. S.; Brandao, P.; Felix, V.; Das, D. Tuning of azine derivatives for selective recognition of Ag plus with the in vitro tracking of endophytic bacteria in rice root tissue. *Dalton Trans.* **2016**, *45*, 19491−19499.

(33) Liu, D.; Yang, X.; Wang, B. Sensing a CO-Releasing Molecule (CORM) Does Not Equate to Sensing CO: The Case of DPHP and CORM-3. *Anal. Chem.* **2023**, *95*, 9083−9089.

(34) Mancuso, C.; Perluigi, M.; Cini, C.; De Marco, C.; Giuffrida Stella, A. M.; Calabrese, V. Heme oxygenase and cyclooxygenase in the central nervous system: A functional interplay. *J. Neurosci. Res.* **2006**, *84*, 1385−1391.

(35) Wang, Y.; Li, B.; Zhang, L.; Liu, L.; Zuo, Q.; Li, P. A highly selective regenerable optical sensor for detection of mercury(II) ion in water using organic−inorganic hybrid nanomaterials containing pyrene. *New J. Chem.* **2010**, *34*, 1946−1953.

(36) Wang, Y.; Li, B.; Zhang, L.; Song, H.; Zhang, L. Targeted Delivery System Based on Magnetic Mesoporous Silica Nanocomposites with Light-Controlled Release Character. *ACS Appl. Mater. Interfaces* **2013**, *5*, 11−15.

(37) Wang, Y.; Li, B.; Liu, Y.; Zhang, L.; Zuo, Q.; Shi, L.; Su, Z. Highly sensitive oxygen sensors based on Cu(I) complex−polystyrene composite nanofibrous membranes prepared by electrospinning. *Chem. Commun.* **2009**, *39*, 5868−5870.

(38) Yang, Y.; Li, B.; Zhang, L.; Li, P.; Jiang, H. Multi-branched triphenylamine−rhodamine derivatives: Synthesis and fluorescent sensing for Cu^{2+} and Hg^{2+} ions. *Talant* **2013**, *115*, 938−942.

(39) Zu, X.; Zhao, Y.; Li, X.; Chen, R.; Shao, W.; Li, L.; Qiao, P.; Yan, W.; Pan, Y.; Xu, Q.; Zhu, J.; Sun, Y.; Xie, Y. Reversible Switching Cu^{II}/Cu^{I} Single Sites Catalyze High-rate and Selective CO_2 Photoreduction. *Angew. Chem., Int. Ed.* **2023**, *62*, No. e202215247.

(40) Bai, C.; Zhang, J.; Qin, Y.; Meng, Q.; Yao, J.; Huang, H.; Wei, B.; Li, R.; Zhang, L.; Miao, H.; Qu, C.; Qiao, R. Strategy for Detecting Carbon Monoxide: Cu^{2+}-Assisted Fluorescent Probe and Its Applications in Biological Imaging. *Anal. Chem.* **2022**, *94*, 11298−11306.